Thermodynamics of energy extraction from fractured hot dry rock

J. S. Lim and A. Bejan
Department of Mechanical Engineering and Materials Science, Duke University, Durham, NC, USA

J. H. Kim
Electric Power Research Institute, Palo Alto, CA, USA

It has been proposed to extract energy from the subterranean hot dry rock bed (HDR) by creating one or more narrow fractures in the rock and circulating cold water through the fractures. In time, the temperature of the rock region surrounding the crack drops under the influence of time-dependent conduction. This study presents the most basic thermodynamic aspects (first law and second law) of the HDR energy extraction process. It shows which parameters most influence the amount of useful energy (exergy) extracted from the HDR reservoir over a fixed time interval. For example, the water flow rate can be selected optimally in order to maximize the delivery of exergy over the lifetime of the HDR system.

Keywords: geothermal energy; hot dry rock; second-law analysis

Introduction

One of the methods for the extraction of geothermal power is the hot dry rock (HDR) system. This method has attracted considerable attention, from analytical studies[1–7] to the construction of experimental wells.[8] The power source in such systems is the solid (dry) rock bed that can be found at 1–3 km underground. The rock temperatures in these regions are in the 200–300°C range.

The simplest HDR system for power extraction has the features illustrated in Figure 1. The rock is first fractured hydraulically[5,8,9] in order to generate a crack through which cold water will later be circulated. The crack is approximated fairly well by a disc with a diameter of the order of 1 km and a thickness of 1 cm or more. The two surfaces of this crack become the heat exchanger area between the hot rock and the cold water that is pumped through the crack. The stream of cold water is pumped down through one well and returns to ground level through a parallel well. The return duct is well insulated in order to prevent the excessive cooling of the hot water produced in the crack.

The productive life span of an HDR system is finite because, in time, the cold water that is circulated through the crack has the effect of lowering the temperature of the two immediate rock layers that sandwich the crack. The purpose of this paper is to demonstrate the existence of an interesting optimal water flow rate for the operation of an HDR system for power production. Consider the idea of extracting the most useful energy (exergy) from the rock over a certain time interval. If the flow rate is sufficiently large, then the water returns to ground level with a temperature that is almost as low as the original inlet temperature. As a consequence, the delivery of exergy (roughly the product of flow rate times temperature rise) is low. In the opposite extreme, where the water flow rate is sufficiently low, the temperature rise is large but finite, because it is limited by the rock temperature, T_∞. The amount of delivered exergy is again low because of the vanishingly small flow rate. There must exist an intermediate flow rate for which the delivery of exergy is maximum.

In what follows, we determine this optimal flow rate and, based on it, the upper thermodynamic limits for the production of useful energy from a given HDR system. The study begins with the simplest possible model, in order to demonstrate analytically the existence of the optimal flow rate and the manner in which the system parameters affect the thermodynamic performance. Later, a sequence of more refined models demonstrate that the optimal flow rate and the trends revealed by the simplest model are correct.

Address reprint requests to Professor Bejan at the Dept. of Mechanical Engineering and Materials Science, Duke University, Durham, NC 27706, USA.

Received 10 April 1991; accepted 29 August 1991

Unidirectional conduction model

A simple model of the heat transfer process during the extraction of energy from the HDR has been constructed in Figure 2. Only one side (the lower side) of the crack is shown. Half of the total water flow rate $\dot{m}$ (constant) is used for cooling, by time-dependent conduction, the rock situated on the lower side of the crack. The rock is modeled as a semi-infinite conducting medium with the temperature $T(y, t)$. The water is modeled as an incompressible liquid with constant c_p. The pressure drop experienced by the water stream through the crack is assumed to be negligible.

In this first model, the longitudinal variation of the water and rock temperatures is neglected by assigning a single temperature, $T_{out}(t)$, to the instantaneous water inventory in the crack. This is equivalent to the assumption that the instantaneous water inventory is very well mixed to a single temperature, which is also equal to the temperature of the

outflowing stream, T_{out}. The water inlet temperature is T_{in}. Treating the control volume swept by the $\dot{m}/2$ stream as an open thermodynamic system, we note that the first law requires

$$\frac{\dot{m}}{2} c_P (T_{out} - T_{in}) = hA(T_0 - T_{out}) \quad (1)$$

In this equation, A is the area swept by the $\dot{m}/2$ stream and h is the average heat transfer coefficient based on A. The rock-stream thermal conductance hA is assumed constant. The temperature of the rock-stream interface is T_0. On the lower side of the rock-stream interface (at $y = 0$) the convective heat flux $h(T_0 - T_{out})$ is matched by the conduction heat flux that arrives from the semi-infinite rock medium,

$$h(T_0 - T_{out}) = k\left(\frac{\partial T}{\partial y}\right)_{y=0} \quad (2)$$

Finally, in any y = constant plane inside the rock, the first law of thermodynamics requires

$$\frac{\partial T}{\partial t} = \alpha \frac{\partial^2 T}{\partial y^2} \quad (3)$$

in which α is the thermal diffusivity of the rock. The rock temperature distribution $T(y, t)$ must satisfy Equation 3, the interface condition 2, the far-field condition

$$T = T_\infty \quad \text{at} \quad y = \infty \quad (4)$$

and the initial condition

$$T = T_\infty \quad \text{at} \quad t = 0 \quad (5)$$

It is useful to nondimensionalize the problem defined between Equations 1–5, by introducing the dimensionless variables

$$\theta = \frac{T - T_{in}}{T_\infty - T_{in}}, \quad \theta_{out} = \frac{T_{out} - T_{in}}{T_\infty - T_{in}}, \quad \theta_0 = \frac{T_0 - T_{in}}{T_\infty - T_{in}} \quad (6)$$

$$\eta = \frac{y}{k/h}, \quad \tau = \frac{t}{k^2/(h^2\alpha)} \quad (7)$$

The dimensionless version of Equations 1–5 is, in order,

$$(1 + M)\theta_{out} = \theta_0 \quad (8)$$

$$\theta_0 - \theta_{out} = \left(\frac{\partial \theta}{\partial \eta}\right)_{\eta=0} \quad (9)$$

$$\frac{\partial \theta}{\partial \tau} = \frac{\partial^2 \theta}{\partial \eta^2} \quad (10)$$

$$\theta = 1 \quad \text{at} \quad \eta = \infty \quad (11)$$

$$\theta = 1 \quad \text{at} \quad \tau = 0 \quad (12)$$

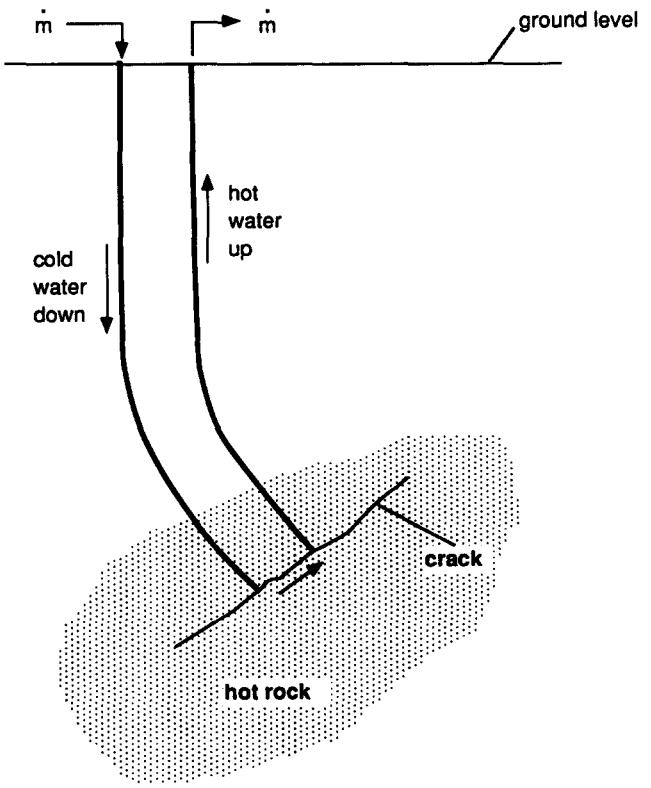

Figure 1 The main components of an HDR system for the extraction of geothermal power

Notation

A	Area of one side of crack
c_P	Water specific heat at constant pressure
$\dot{E}_x$	Rate of exergy delivery, Equation 20
E_x	Total exergy delivery, Equation 21
$\tilde{E}_x$	Dimensionless total exergy delivery, Equation 23
h	Heat transfer coefficient
k	Rock thermal conductivity
k_w	Water thermal conductivity
L	Swept length of crack
$\dot{m}$	Water flow rate
M	Dimensionless flow rate, Equation 13
n	Number of grid point in the η direction
p	Wetted perimeter
t	Time
t_{end}	Total duration of the extraction process
T	Absolute temperature
T_f	Water temperature
T_{in}	Water inlet temperature
T_{out}	Water outlet temperature
T_0	Crack surface temperature
T_∞	Far-field rock temperature
x, y	Cartesian coordinates, Figures 2 and 5

Greek symbols

α	Rock thermal diffusivity
α_η	Rate of grid stretching, Equation 33
δ	Conduction boundary-layer thickness
ε	Temperature span parameter, Equation 25
η	Dimensionless transversal coordinate, Equation 7
θ	Dimensionless rock temperature, Equation 6
θ_f	Dimensionless water temperature
θ_{out}	Dimensionless outlet temperature, Equation 6
θ_0	Dimensionless surface temperature, Equation 6
ξ	Dimensionless longitudinal coordinate, Equation 29
τ	Dimensionless time, Equation 7
τ_{end}	Dimensionless total duration of the extraction process, Equation 7, with $t = t_{end}$

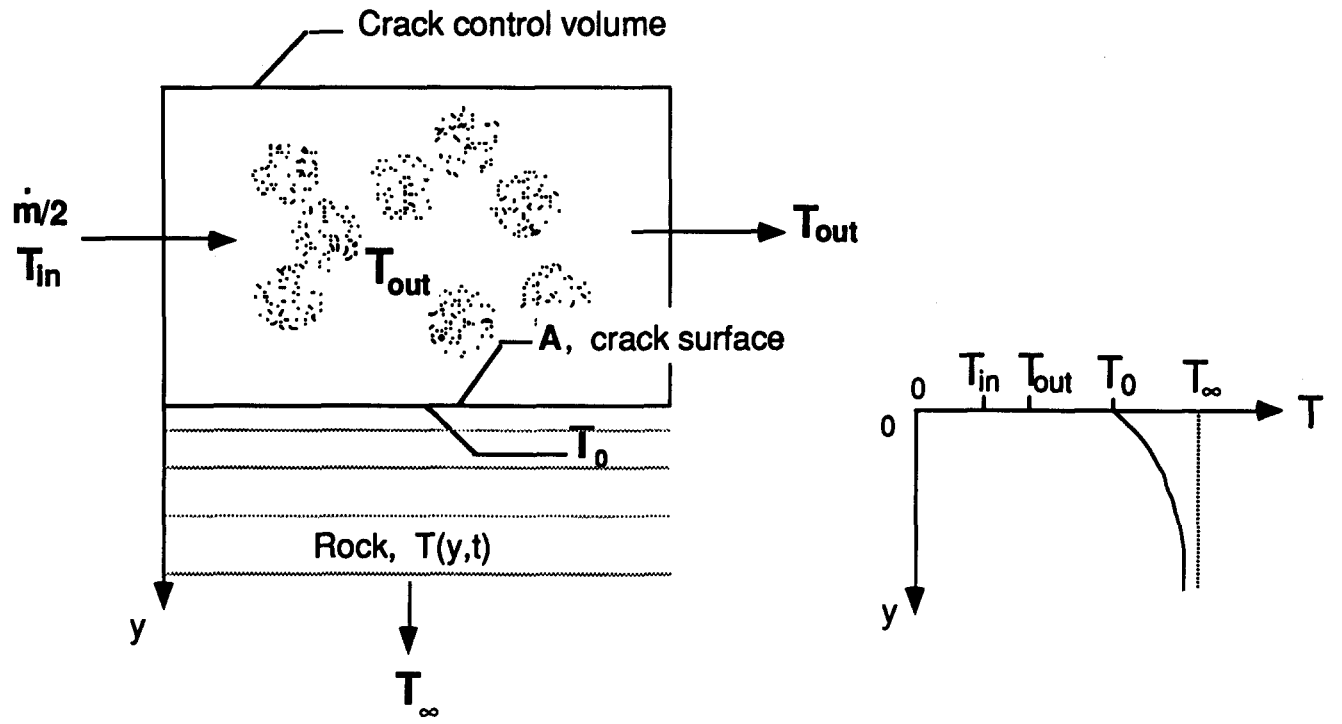

Figure 2 Unidirectional time-dependent conduction model for the heat transfer in the rock on one side of the crack

where M is the dimensionless mass flow rate

$$M = \frac{(\dot{m}/2)c_P}{hA} \tag{13}$$

The approximate behavior of the temperature distribution in the HDR system can be determined analytically by assuming a rock temperature profile that resembles the one sketched on the right side of Figure 2:

$$\theta = (\theta_0 - 1)\exp\left(-\frac{\eta}{\delta}\right) + 1 \tag{14}$$

The function $\delta(\tau)$ is the dimensionless thickness of the conduction boundary layer that forms between the T_0 interface and the T_∞ far field. Substituting the temperature profile 14 in Equations 9 and 10, and integrating from $\eta = 0$ to $\eta = \infty$ we obtain

$$\theta_0 - \theta_{out} = \frac{1 - \theta_0}{\delta} \tag{15}$$

$$\frac{d}{d\tau}[(1 - \theta_0)\delta] = \frac{1 - \theta_0}{\delta} \tag{16}$$

Equations 8, 15, and 16 can be solved analytically for θ_0, θ_{out}, and δ as functions of time (τ) and flow rate (M). The solution is given implicitly by the following sequence:

$$\tfrac{1}{2}(\theta_0^{-2} - 1) + \ln\theta_0 = \left(\frac{M}{1 + M}\right)^2 \tau \tag{17}$$

$$\theta_{out} = \frac{\theta_0}{1 + M} \tag{18}$$

$$\delta = \left(\frac{1}{\theta_0} - 1\right)\left(\frac{1}{M} + 1\right) \tag{19}$$

and is presented graphically in Figure 3. The interface temperature θ_0 decreases monotonically as both τ and M increase. The temperature of the crack fluid exhibits a similar behavior, although it is generally lower than the interface temperature shown in the upper graph of Figure 3. Finally, the bottom graph of Figure 3 shows that the thickness of the conduction boundary layer increases approximately as $\tau^{1/2}$, which is the expected behavior in unidirectional time-dependent conduction. The mass flow rate number has a negligible effect on $\delta(t)$ in the M range 1–10.

Maximum exergy delivery

Of primary interest in the field of energy engineering is the extraction of potentially useful energy (exergy) from the HDR system. The instantaneous rate at which the $\dot{m}/2$ stream extracts exergy from the crack control volume of Figure 2 is

$$\dot{E}_x = \frac{\dot{m}}{2} c_P\left(T_{out} - T_{in} - T_{in}\ln\frac{T_{out}}{T_{in}}\right) \tag{20}$$

It is assumed that the absolute inlet temperature T_{in} is equal to the atmospheric (environmental) temperature from which the water stream originates. The group in the round brackets times c_P is the specific flow exergy of isobaric water as an incompressible liquid,[10] relative to the environment of temperature T_{in}. The total exergy extracted by the $\dot{m}/2$ stream during the time interval $0 - t_{end}$ is

$$E_x = \int_0^{t_{end}} \dot{E}_x\, dt \tag{21}$$

or, in terms of the dimensionless variable defined in Equations 6, 7, and 13,

$$E_x = \int_0^{\tau_{end}} M[\varepsilon\theta_{out} - \ln(1 + \varepsilon\theta_{out})]\, d\tau \tag{22}$$

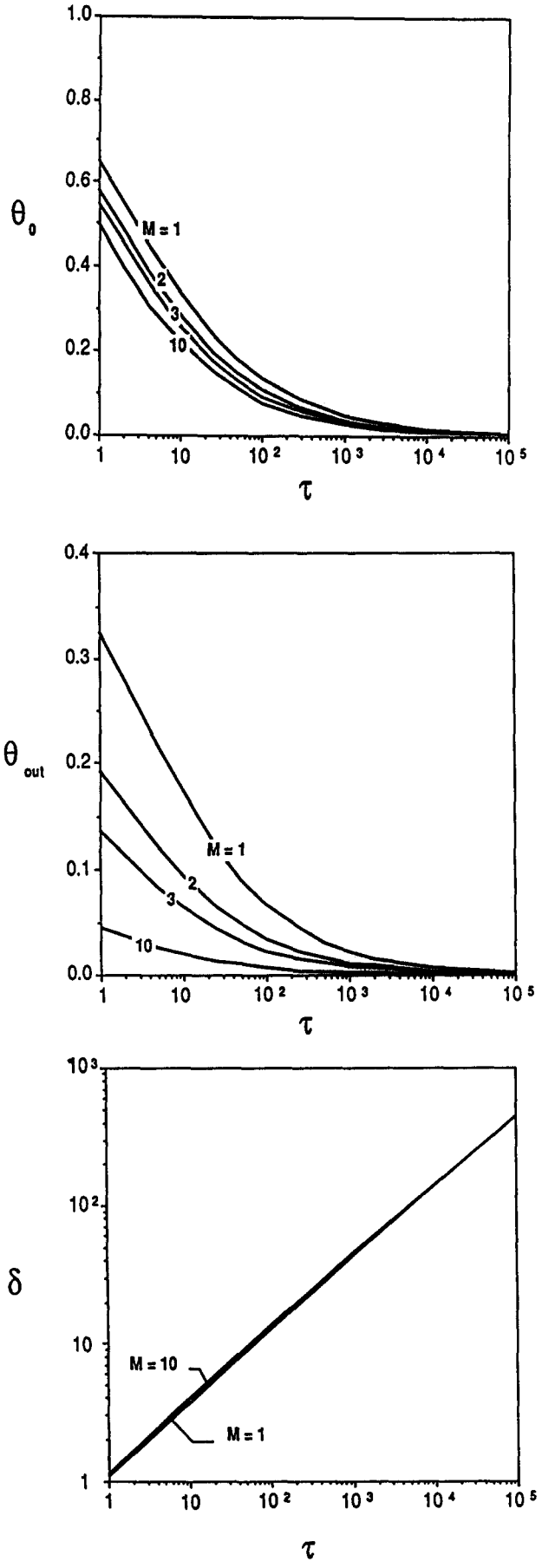

where

$$\tilde{E}_x = \frac{E_x}{AT_{in}k^2/(h\alpha)}, \qquad \tau_{end} = \frac{t_{end}}{k^2/(h^2\alpha)}, \qquad \varepsilon = \frac{T_\infty}{T_{in}} - 1 \tag{23-25}$$

In Equations 20, 23, and 25, all the temperatures are thermodynamic temperatures expressed in degrees Kelvin. This is why with $T_{in} \sim 300$ K and $T_\infty \sim 400$ K, the dimensionless temperature span parameter ε can be expected to be of order 1 or smaller.

The time t_{end} represents the entire duration of the exergy extraction phase—the life of this particular HDR well. The order of magnitude of the dimensionless time τ_{end} can be estimated by using Equation 24 with $t_{end} \sim 1$ year, the properties of granite $\alpha = 0.012$ cm^2/s and $k = 2.9$ W/m·K, and a heat transfer coefficient of order $h \sim k_w/D$, where $k_w \sim 0.7$ W/m·K is the conductivity of water, and $D \sim 0.5$ cm is the crack width. The result of this order of magnitude calculation is $\tau_{end} \sim 10^5$.

The dimensionless exergy delivery, $\tilde{E}_x$, is a function of τ_{end}, M, and ε. Figure 4 (top) shows the influence of τ_{end} and M when the temperature span parameter is fixed, $\varepsilon = 1$. The most interesting aspect of this result is that it reveals the optimal flow rate (M_{opt}) that maximizes the total exergy delivery when the life of the well is fixed. The total exergy decreases to zero in the limit $M \to 0$, because in that limit the communication between the HDR and the user disappears. The exergy $\tilde{E}_x$ decreases again in the limit $M \to \infty$, because in the presence of an excessive flow rate the rock cools very fast, and during most of the time period t_{end} the stream experiences a negligible temperature rise while flowing through the crack.

Figure 4 (middle) shows the optimal mass flow rate number obtained numerically by maximizing the total exergy delivery, $\tilde{E}_x$, subject to a fixed time interval, τ_{end}. There is one $M_{opt}(\tau_{end})$ curve for each set of extreme temperatures (T_∞, T_{in}), i.e., for each value of ε. The optimal flow rate decreases monotonically as the overall duration of the extraction process increases. In conclusion, for maximum exergy extraction, a well that is operated for only 6 months should have a higher flow rate than a well whose operation will last 5 years.

The monotonic relationship between M_{opt} and τ_{end} revealed in Figure 4 (middle) may seem to contradict the constant-M assumption made in the model described in Section 2. In fact, there is no contradiction because the flow rate M is constant (time-independent) throughout the life of the process 0–τ_{end}. Only when M happens to be equal to the optimal flow rate M_{opt} identified in Figure 4 (middle) does the total exergy delivery integrated from $\tau = 0$ to $\tau = \tau_{end}$ reach its maximum value.

That maximum amount of delivered exergy is summarized in Figure 4 (bottom), as a function of τ_{end} and ε. This amount increases monotonically with the duration of the exergy extraction phase, τ_{end}; however, this increase is much slower than a simple proportionality between $\tilde{E}_{x,max}$ and τ_{end}. The effect of the temperature span parameter ε is also illustrated in Figure 4 (bottom). The exergy delivery maximum decreases monotonically as ε decreases.

Numerical solution

The preceding results were based on the integral solution that was developed for the heat transfer (first law) part of the

Figure 3 The integral solution to the problem of Figure 2. (Top) Interface temperature. (Middle) Mixed stream temperature. (Bottom) Thickness of the rock conduction boundary layer

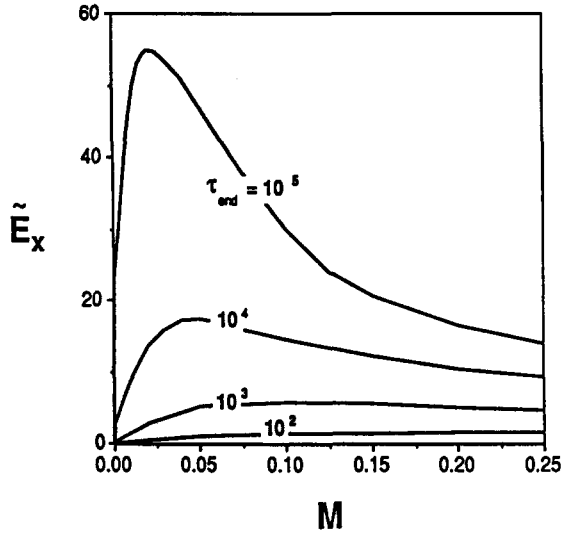

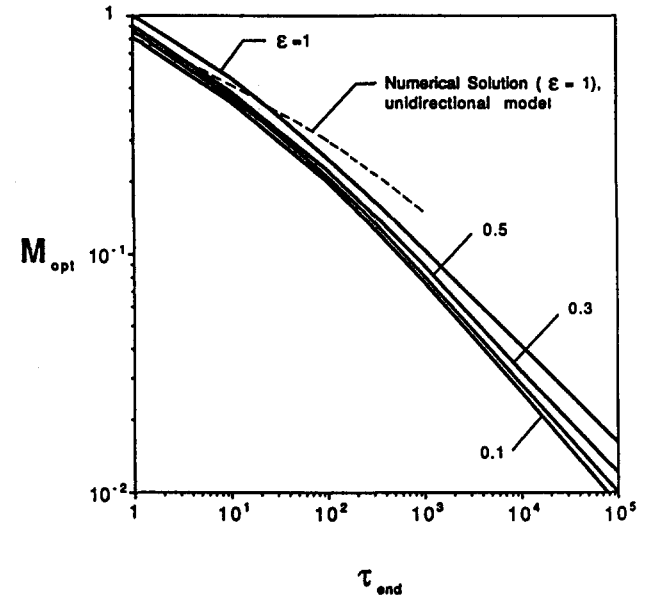

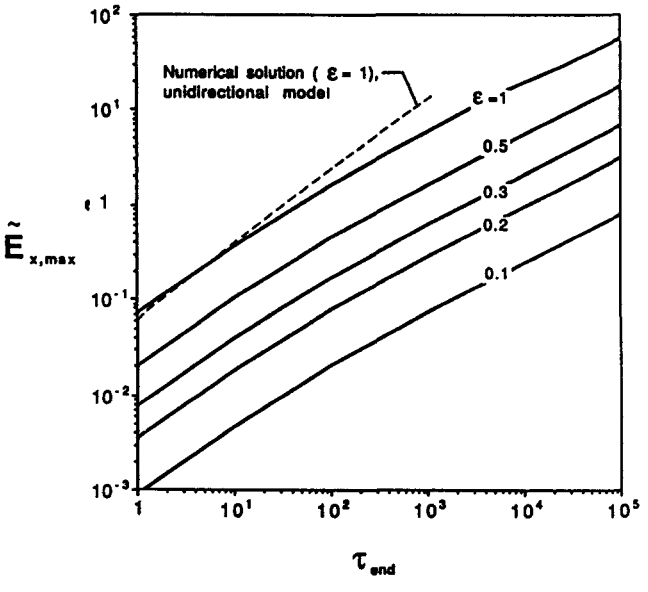

problem defined in Figure 2. In order to check the validity of the integral solution and the subsequent thermodynamic conclusions (Figure 4), we solved the same heat transfer problem numerically for the temperature distribution in the rock bed $\theta(\eta, \tau)$.

The numerical work consisted of solving Equations 8–12, starting from the initial condition

$$\theta = 1 \quad \text{at} \quad \tau = 0 \tag{26}$$

The algorithm was based on the simple explicit method and on forward difference approximations. Table 1 shows the effect of grid size on the optimal flow rate for the period $\tau_{end} = 10^3$. The following results are based on the grid listed in the bottom line of the table.

The dashed line in Figure 4 (middle) shows a comparison between the optimal flow rate based on the numerical solution and the one based on the integral solution (solid line). The numerical M_{opt} curve ends at $\tau_{end} = 10^3$ because for greater τ_{end} values the computational cost became prohibitive. This comparison demonstrates that the integral solution provides an adequate order of magnitude estimate for M_{opt}, and that the relationship between M_{opt} and τ_{end} indeed has the character of the solid-line curve revealed first by the integral solution.

A similar comparison has been constructed in Figure 4 (bottom) for the maximum exergy delivery that corresponds to the M_{opt} and τ_{end} values of Figure 4 (middle). The numerical solution (dashed line) agrees in an order of magnitude sense with the integral solution, especially at small values of τ_{end}. In the opposite direction, the integral solution consistently underpredicts the $\tilde{E}_{x,max}$ values calculated numerically. The general behavior of the $\tilde{E}_{x,max}$ function is the same as in the integral solution: the maximum exergy delivery increases monotonically with the extraction period τ_{end}.

Two-dimensional conduction model

One respect in which the simple model of Figure 2 can be improved is by dropping the assumption that the water stream is well mixed inside the crack. Since the crack spacing is of the order of 1 cm (i.e., not a wide cavity), it makes sense to assume that the water temperature varies between its inlet ($x = 0$) and outlet ($x = L$). This new model is presented in Figure 5. Because of the longitudinal variation of the water bulk temperature $T_f(x, t)$, the instantaneous temperature of the rock T depends on both x and y.

The new set of governing equations consists of

$$\dot{m}c_p \frac{\partial T_f}{\partial x} = hp(T_0 - T_f) \tag{27}$$

Table 1 The effect of grid size on the accuracy of the numerical solution ($\varepsilon = 1$, $\tau_{end} = 10^3$)

Nodes in the η direction	$\Delta\eta$	$\Delta\tau$	CPU (s)	M_{opt}
50	0.2	0.02	4	0.269
200	0.1	0.005	49	0.167
400	0.05	0.00125	389	0.161

Figure 4 (Top) The effect of flow rate (M) and extraction period (τ_{end}) on the total amount of delivered exergy ($\varepsilon = 1$). (Middle) The optimal flow rate for maximum τ_{end}-integrated exergy delivery. (Bottom) The effect of the extraction period (τ_{end}) and temperature span (ε) on the maximum exergy delivery

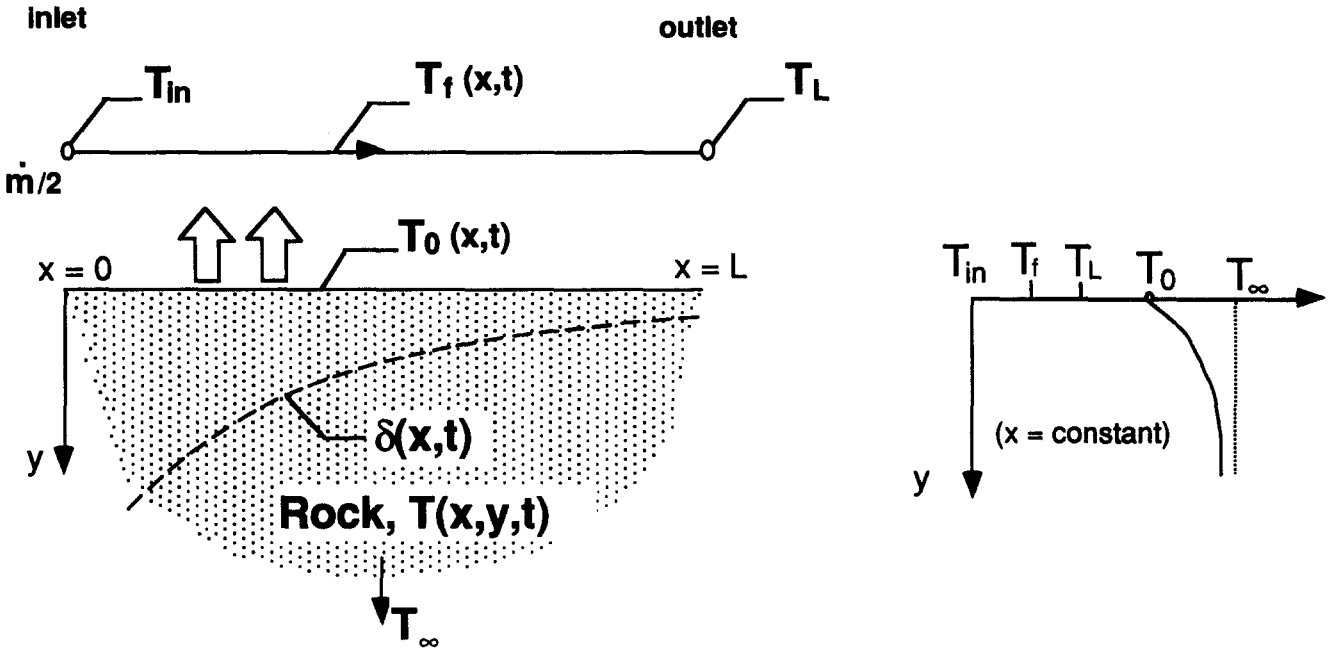

Figure 5 Bidirectional time-dependent conduction model for the heat transfer in the rock on one side of the crack

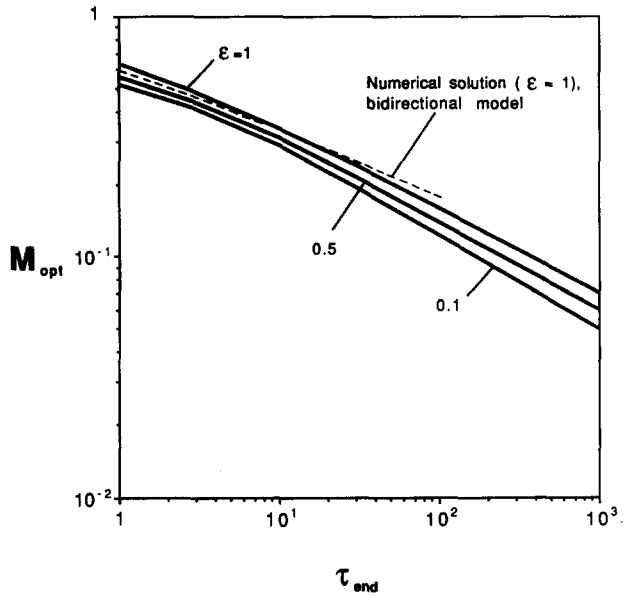

Figure 6 The optimal flow rate based on the model of Figure 5

$$h(T_0 - T_f) = k\left(\frac{\partial T}{\partial y}\right)_{y=0} \tag{28}$$

and the conduction Equation 3, in which $T = T(x, y, t)$. Note the use of p for the wetted perimeter of the crack surface, or $p = A/L$. The rock temperature must satisfy the far-field condition 4 and the initial condition 5.

These governing equations can be nondimensionalized by using the variables of Equations 6 and 7 and the longitudinal position

$$\xi = \frac{x}{\frac{1}{2}\dot{m}c_p/(hp)} \tag{29}$$

Note that $\xi = 1/M$ at the end of the crack ($x = L$). The dimensionless equations are Equation 10, in which $\theta(\xi, \eta, \tau)$ and

$$\frac{\partial \theta_f}{\partial \xi} = \theta_0 - \theta_f \tag{30}$$

$$\theta_0 - \theta_f = \left(\frac{\partial \theta}{\partial \eta}\right)_{\eta=0} \tag{31}$$

where $\theta_f = (T_f - T_{in})/(T_\infty - T_{in})$. These equations were solved by two methods, integral and numerical, in ways that parallel the work presented in the preceding sections of this paper.

Integral solution

The analysis involved the use of a conduction boundary-layer thickness function that is a function of both time and longitudinal position, $\delta(\xi, \tau)$. The shape of the rock temperature variation in η was approximated by an exponential, and the conduction equation was integrated from $\eta = 0$ to $\eta = \infty$. Numerical results were developed for $\delta(\xi, \tau)$, $\theta_0(\xi, \tau)$ and $\theta_f(\xi, \tau)$; however, the details of the procedure are omitted in the interest of brevity. The results were then substituted in the exergy delivery function, which was later maximized with respect to M.

The solid lines in Figure 6 show the optimal flow rate M_{opt} in the τ_{end} range 1–10^3. These results are very close to those produced by the simpler model in Figure 4 (middle). Indeed, if the $\varepsilon = 1$ curve of Figure 6 is added to Figure 4 (middle), its position will be a bit under the two intersecting curves that are shown already in Figure 4 (middle).

Numerical solution

The dimensionless problem stated earlier in this section was solved numerically based on finite-difference approximations of the governing equations. The grid was nonuniform in the η

Table 2 The effect of grid size on the accuracy of the numerical solution ($\varepsilon = 1$, $\tau_{end} = 10^2$)

Nodes in the η direction	$\Delta\eta$	$\Delta\xi$	$\Delta\tau$	CPU (s)	M_{opt}
50	0.2	0.1	0.02	14	0.230
100	0.1	0.05	0.005	237	0.185
200	0.05	0.05	0.00125	1328	0.179

direction,

$$\eta_i = \eta_1 \alpha_\eta^{i-1} \tag{32}$$

in which η_i is the η location of the i^{th} grid line, η_1 is the first grid line (the smallest step in η), and α_η is the rate of grid stretching,

$$\eta_{max} = \frac{\eta_1(1-\alpha_\eta^n)}{1-\alpha_\eta} \tag{33}$$

In this last expression, η_{max}, and n are the size of the computational domain in the η direction and the number of nodes in that direction. These were selected based on the accuracy tests sampled in Table 2. The final choice is listed in the last line of the table.

The numerical version of the $M_{opt}(\tau_{end})$ curve was plotted as a dashed line next to the integral version in Figure 6. Computational costs did not permit the plotting of the numerical curve beyond $\tau_{end} = 10^2$. The excellent agreement between the two curves lends confidence to the integral solution that extends to $\tau_{end} = 10^3$. The agreement between Figure 6 and the corresponding figure produced by the much simpler model of Figure 2, lends confidence in those earlier results, which covered the wider τ_{end} range of 1–10^5.

Conclusion

In this study we have considered the most basic thermodynamic aspects of the extraction of useful energy from an HDR reservoir. The combined first-law and second-law analysis showed the manner in which the thermodynamic performance depends on the key physical parameters of the system. These trends were established first by using a very simple model; later, they were confirmed by more refined analyses.

A key feature of the thermodynamic limits to HDR exergy extraction is the existence of an optimal water flow rate. The study documented the relationship between the system parameters and the optimal flow rate and corresponding maximum exergy delivery.

It is important to note that the reason for the emergence of the optimal flow rate in the present analysis is our assumption (modeling decision) that the rock–water heat transfer coefficient is finite (finite h in Equation 1, or finite M in Equation 13). The previous heat transfer (first law) analyses of the water cooled crack[1–7] relied on the assumption that the water bulk temperature is mathematically equal to the crack surface temperature. In terms of the present notation, the older analyses correspond strictly to the case $M = 0$ (i.e., infinite heat transfer coefficient).

In order to illustrate the relevance of the finite-h assumption, consider the numerical example exhibited by Gringarten et al.[3] The crack has an area $A \sim 1\ km^2$, and a water flow rate of 100 kg/s. Assuming $D \sim 1$ cm for the crack spacing (e.g., Abé and Hayashi[11]), and recognizing $h \sim k_w/D$ as the laminar-flow scale of the heat transfer coefficient, the scale of the dimensionless mass flow rate (13) turns out to be $M \sim 10^{-2}$.

Continuing with the same numerical example, and using the k and α of granite, we find that the dimensionless time (7) that corresponds to an extraction period of 20 years has the order of magnitude $\tau_{end} \sim 10^5$. A reexamination of Figure 4 (top and middle) shows that this numerical example (M, τ_{end}) is covered by the present analysis. Coincidentally, Figure 4 (middle) shows that the flow rate postulated in the numerical example ($M \sim 10^{-2}$) is close to the optimal flow rate that corresponds to the extraction period $\tau_{end} \sim 10^5$.

It should be noted that the crack spacing scale D has a profound effect on numerical calculations of the type exhibited in the preceding paragraph. For example, in the beginning of the energy extraction process the more appropriate scale is $D \sim 1$ mm, and this would yield $M \sim 10^{-5}$ and $\tau_{end} \sim 10^8$. As the cooling of the HDR progresses, rock contracts and D increases to $D \sim 1$ cm and even larger spacings,[11] justifying the numerical example given in the preceding paragraphs.

The optimal flow rate for an HDR system is the latest example that there exists *optimal ways of designing time-dependent cooling or heating processes and devices*. This is an important development in modern engineering thermodynamics. Previous examples of such optimal process histories referred to the heating or cooling of a thermal mass (e.g., solid block) to a given temperature during a given time interval. This progress was reviewed elsewhere.[10]

Acknowledgment

This work was sponsored by the Electric Power Research Institute through Contract No. RP 8006-04.

References

1 Bodvarsson, G. On the temperature of water flowing through fractures. *Journal of Geophysical Research*, 1969, **74**, 1987–1992

2 Bodvarsson, G. An estimate of the natural heat resources in a thermal area in Iceland. *Geothermics*, 1970, Special Issue 2, **2**, Part 2, 1289–1298

3 Gringarten, A. D., Witherspoon, P. A. and Ohnishi, Y. Theory of heat extraction from fractured hot dry rock. *Journal of Geophysical Research*, 1975, **80**, 1120–1124

4 Lowell, R. P. Comments on 'Theory of heat extraction from fractured hot dry rock.' *Journal of Geophysical Research*, 1976, **81**, 359

5 Abé, H., Keer, L. M. and Mura, T. Theoretical study of hydraulically fractured penny-shaped cracks in hot, dry rocks. *International Journal for Numerical and Analytical Methods in Geomechanics*, 1979, **3**, 79–96

6 Abé, H., Sekine, H. and Shibuya, Y. Thermoelastic analysis of a cracklike reservoir in a hot dry rock during extraction of geothermal energy. *Journal of Energy Resources Technology*, 1983, **105**, 503–508

7 Shibuya, Y., Sekine, H. and Takahashi, Y. Some results being used to stable control of an artificial geothermal crack in a hot dry rock. *International Symposium on Geothermal Energy*, Kumamoto and Beppu, Japan, November 10–14, 1988, 485–488

8 Abé, H. Design of HDR reservoir—an overview of Γ-project. *Proc. Int. Workshop on Hot Dry Rock*, Tsukuba, Japan, November 4–5, 1988

9 Abé, H., Mura, T. and Keer, L. M. Growth rate of a penny-shaped crack in hydraulic fracturing rocks. *Journal of Geophysical Research*, 1976, **81**, 5335–5340

10 Bejan, A. *Advanced Engineering Thermodynamics*. Wiley, New York, 1988, 135, 651–654

11 Abé, H. and Hayashi, K. Artificial subsurface cracks and geothermal energy. *JSME International Journal*, 1988, **31**, 1–11